Absolute densities of energetic hydrogen ion species in an abnormal hollow cathode discharge

J. Kipritidis,* J. Khachan, M. Fitzgerald, and O. Shrier
School of Physics, University of Sydney, Sydney 2006, Australia

(Received 6 December 2007; revised manuscript received 14 April 2008; published 12 June 2008)

We develop an optical measurement for densities of fast (units to tens of keV) hydrogen ions in an abnormal hollow cathode discharge in units to tens of mTorr pressure range. This method combines results from previous collisional-radiative models, comparing the intensity of Balmer H_α due to dissociative excitation of H_2 by fast electrons to Doppler-shifted emission arising from charge exchange of energetic ions. The method requires only two inputs: the current density due to fast electrons and a single H_α spectrum of the characteristic emission channel at the anode. We model in particular the cylindrical interelectrode discharge of an inertial electrostatic confinement device. Experimentally, we find that the density of fast ions emerging from the cathode (bias −5 kV at 20 mTorr) is in the order 10^{14} m^{-3}, increasing approximately linearly with current in the 10–30 mA range. Calculated densities agree with values obtained in similar apparatus using Langmuir probes and analysis of dust particle motion.

DOI: 10.1103/PhysRevE.77.066405 PACS number(s): 52.59.−f, 52.70.−m, 32.30.−r, 32.70.Fw

I. INTRODUCTION

For pressures of tenths to units of Torr, Balmer H_α emission has long been linked to the study of fast excited H atoms in a hollow cathode hydrogen glow discharge [1,2]. The electrode geometry of Fig. 1 depicts a simple case, with an open-ended and cylindrically symmetric cathode sitting within a spherical and grounded anode grid. At units to tens of mTorr pressures and with a cathode bias of units to tens of kilovolts, the voltage is observed to rise rapidly with current. This "abnormal" hollow cathode discharge is characterized by channels of brilliant optical emission emerging from the cathode apertures [3–5]. Figure 2 depicts a typical H_α spectrum viewed parallel to the discharge axis through the center of the cathode. The line shape consists of a Lorentzian peak (with an intensity maximum at wavelength $\lambda_0 \sim 6563$ Å) flanked by Doppler-shifted wings. In this work, we combine our knowledge of the respective emission processes, calculating in absolute terms the densities of energetic ions emerging from the cathode.

Appealing to previous studies of H_α emission in a 1–2 Torr abnormal glow discharge [6] as well as lower pressure (0.01–0.1 Torr) parallel-plate rf [7] and dc [8] discharges, we attribute the central peak to the dissociative excitation of H_2 by fast (units of keV) electrons. This produces excited $H(n,l)$ through the reaction

$$e^- + H_2 \rightarrow e^- + H_2^* \rightarrow e^- + H(1,s) + H(n,l), \tag{1}$$

with n and l denoting principal and orbital quantum numbers. The primary deexcitation mechanism is spontaneous emission, wherein the kinetic energy K of an emitting neutral is related to the Doppler shift $\Delta\lambda$ through

$$K = \frac{mc^2(\Delta\lambda)^2}{2\lambda_0^2 \cos^2\theta}, \tag{2}$$

where m is the particle mass, c is the speed of light, and θ is the angle between the particle trajectory and the observation axis. Without applying a deconvolution procedure, the central peak typically has an apparent full width at half-maximum (FWHM) in the order 0.5–1 Å ($K \leqslant 1$–10 eV); here we say dissociative excitation produces "slow" H.

The far wings, on the other hand, have Doppler shifts $\Delta\lambda \geqslant 1$ Å. These have been shown [3] to arise primarily through the charge exchange of energetic (units of keV) hydrogen ions with the background gas. In the mTorr pressure range, the dominant processes are

$$H^+ + H_2 \rightarrow H(n,l) + H_2^+, \tag{3}$$

$$H_2^+ + H_2 \rightarrow H(n,l) + H(1s) + H_2^+, \tag{4}$$

$$H_3^+ + H_2 \rightarrow H(n,l) + H_2 + H_2^+. \tag{5}$$

Here the product neutrals ("fast" H) possess the trajectory of the incident ions, with the incident energy partitioned among product neutrals according to their mass [9]. It follows that the Doppler peak positions characterize the energies and tra-

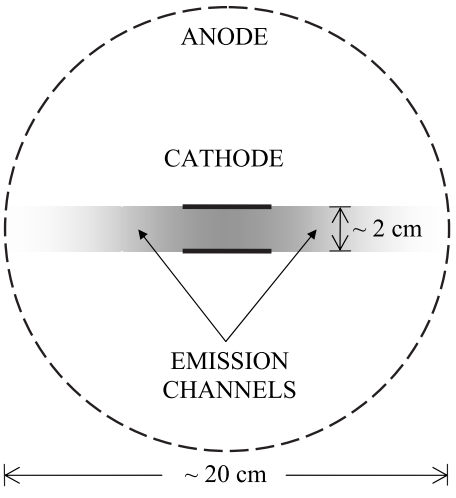

FIG. 1. Schematic diagram of an abnormal hollow cathode discharge. The anode is a grounded spherical mesh, the cathode an open-ended, stainless steel cylinder.

*johnk@physics.usyd.edu.au

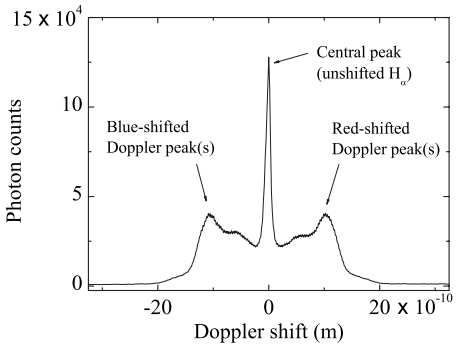

FIG. 2. Typical spectrum of H_α viewed parallel to the discharge axis of Fig. 1. We label the central ("unshifted") peak as well as the blue- and redshifted Doppler wings.

jectories of incident ions, with an increase in emission wavelength or "redshift" arising from ions headed away from the detector. In particular, electron-atom and atom-gas excitations of fast neutrals are neglected on the basis that they cannot account for the previously observed proportionality between fast neutral energies and cathode bias [3]. Indeed, for the discharge of Fig. 1 it has been shown [3–5] that the Doppler-shifted wings are each comprised of three smaller peaks arising from distinct monoenergetic populations of fast H produced in the three charge-exchange processes.

The processes of charge exchange and dissociative excitation have each been the subject of separate collisional-radiative (CR) models for H_α emission applicable to the interelectrode discharge of Fig. 1. CR modeling involves the solution of coupled rate equations governing the populations of atomic energy levels dominated by collisional and radiative transitions [10]. Respectively, the models for dissociative excitation [11] and charge exchange [5] yield information about electron energies and relative densities of energetic ion species. But nowhere has a CR model treated the ratio of shifted-to-unshifted emission in a single spectrum of H_α $(n=3\rightarrow 2)$. Here we relate the two models in order to develop an optical method for measuring absolute densities of energetic hydrogen ions emerging from the cathode.

Our method implicitly calibrates the detector by relating intensity ratios of central and Doppler-shifted H_α peaks measured at an anode several centimeters from the cathode, to the densities of fast and slow excited H (also at the anode). The density of fast excited H at the anode is related to their density at the cathode by radiative decay constants, and subsequently to the densities of fast ions emerging from the cathode through known charge-exchange rate coefficients. Similarly, rate coefficients for dissociative excitation allow us to relate the densities of slow excited H and fast electrons at the anode, the latter of which is estimated using the measured cathode current. It should be noted that the resulting calculation of absolute fast ion densities at the cathode cannot be obtained by considering either of the earlier CR models in isolation.

In particular, we model the interelectrode discharge of Fig. 1 as it pertains to a cylindrically symmetric inertial electrostatic confinement (IEC) device. In its conventional form [12], IEC aims to accelerate ions of a plasma (usually D_2) through concentric gridded electrodes so that populations of monoenergetic nuclei will undergo nuclear fusion reactions within the center. In fact, recent Doppler spectroscopy [13] and numerical modeling [14] at mTorr pressures challenge the argument that energetic ions are confined at all. Here the shift $\Delta\lambda$ of the Doppler peaks increases with distance from the cathode center, implying that the majority of ions are produced within the cathode and undergo charge exchange as they accelerate outward from a central region of positive space charge or "virtual anode." The existence of such a virtual anode is supported by Langmuir probe measurements of electric potential in a similar apparatus [4].

We posit that the virtual anode may be modeled by including ion bombardment of the cathode interior surface as one of the production mechanisms for low-energy secondary electrons. In this picture, the density of low-energy ions is a maximum at the cathode center due to ionizing collisions of electrons oscillating radially within the cathode electric field (the "Pendel" effect). In particular, we expect a steady-state solution as some fraction of diffusing ions are responsible for producing secondary electrons at the wall. This would be quite distinct to the backscattering of ions, a mechanism responsible for production of energetic neutrals diverging from a hollow cathode wall [6]. We stress, however, that such speculation is not the emphasis of this work, which aims to develop a plasma diagnostic based on the earlier semiempirical findings.

In this paper, we develop an optical diagnostic for absolute densities of fast ions for the IEC apparatus described in Sec. II. Section III provides the underlying theory for a cylindrically symmetric discharge of hydrogen, and Sec. IV presents density measurements obtained experimentally.

II. EXPERIMENTAL SETUP

Figure 3(a) depicts the electrode arrangement used for generation of the discharge modeled in Sec. III. The cathode is a segmented stainless steel cylinder of axial length 4.1 cm and major radius 1 cm, and is connected to an external dc power supply providing a bias of units to tens of kV at currents of units to tens of mA.

For the emission channel of interest, we use an anode ring of diameter 3 cm and cylindrical length $\sim$1 cm. The axial separation between edges of the cathode and anode is 6 cm. We extend the discharge to the opposite side using a hemispherical anode mesh of diameter 16 cm. Each point on the mesh is approximately 6 cm from the nearest cathode edge.

For the experiments in Sec. IV, the cathode bias, current, and gas pressure were all measured directly. Cathode bias was measured using a high voltage probe, current was displayed on the power supply, and pressure was read from a Pirani gauge accurate to 10^{-4} Torr. The experimental error for each of these quantities is in the order 5%.

The discharge was observed at an angle $\theta=25°$ to the emission channel at the anode [Fig. 3(b)], using an arrangement of mirrors and a lens for sampling particular positions along the beam. Uncertainty in the lens focal length introduced an error $\sim$1 cm in the sampling position parallel to the discharge axis. We choose to sample the spectrum at the

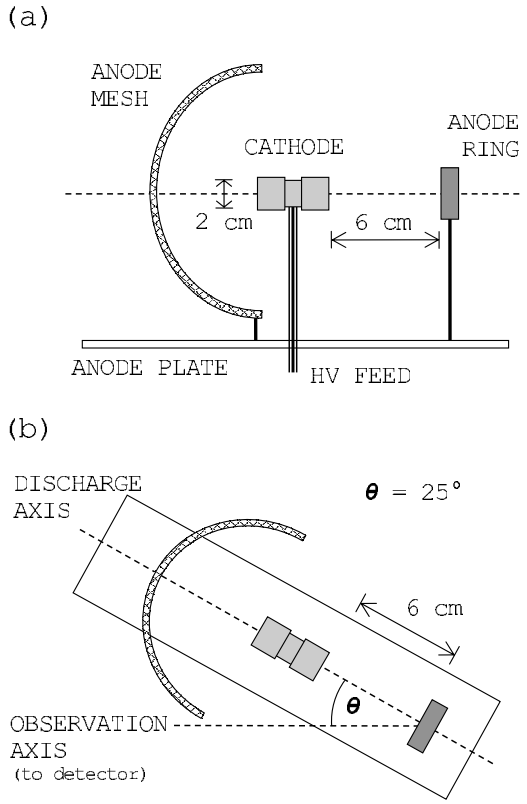

FIG. 3. (a) Schematic diagram of the electrode arrangement used in this study (side-on view). Dimensions are given in the text, with the dashed line indicating the discharge axis. HV denotes high voltage. (b) Electrode arrangement (top-down view), showing the orientation between the discharge and observation axes. The detector is situated outside the vacuum chamber. Note that (a) and (b) share the same scale.

anode as the electron energies there are known (see Sec. III B), whereas the observation angle was chosen so as to provide a clear line of sight through the anode. In general, the angle may be chosen arbitrarily; however, by Eq. (2) a more acute angle ensures a clearer separation between unshifted and Doppler-shifted peaks. The detector was a Princeton Applied Research 1421G linear diode array (LDA) mounted on a 0.5 m focal length Spex 500M monochromator. The resolution (full width at half-maximum) of the setup was ~0.8 Å, with a wavelength separation 0.16 Å between adjacent pixels of the output. The LDA assembly was cooled to 0–5 °C by a Peltier cooler in order to reduce thermal noise.

III. THEORY: SPECTROSCOPIC DETERMINATION OF DENSITIES OF FAST IONS EMERGING FROM THE CATHODE

The CR models for charge exchange and dissociative excitation are described here in detail. We apply these models in relating central and Doppler-shifted H_α emission a distance several centimeters away from the cathode edge, proposing an optical measurement for densities of fast ions emerging from the cathode.

A. CR model for fast excited H produced by charge exchange

In Ref. [5], the CR model for charge exchange resulting in fast atomic $H(n,l)$ consisted of the following set of rate equations:

$$\frac{dn_{H^x_{fast}(n,l)}}{dt} = n_{H_x^+} n_{H_2} k_x(n,l) - \sum_{\substack{(n',l')<(n,l) \\ \text{allowed}}} A_{(n,l)\to(n',l')} n_{H^x_{fast}(n,l)} - k_Q(n,l) n_{H_2} n_{H^x_{fast}(n,l)}. \quad (6)$$

Here $n_{H^x_{fast}(n,l)}$ is the number density of fast atomic H in the excited state (n,l) produced by energetic ions H_x^+ with $x=1,2,3$. Similarly n_{H_2} is the density of background gas and $n_{H_x^+}$ the ion density. For fast atomic $H(3s)$, we would therefore have three equations, one for each Doppler-shifted peak. Background H_2 is assumed to have temperature $T_{H_2}=300$ K, so that H_2 density may be obtained from the ideal gas law.

In our experimental apparatus, a steady-state solution is appropriate and so the left-hand side of Eq. (6) is set to zero. On the right-hand side, the first term gives the contribution of charge exchanging H_x^+ to the population of $H^x_{fast}(n,l)$. For charge exchange, the rate coefficient is k_x, which has units $m^3\ s^{-1}$. The second and third terms describe the deexcitation processes, respectively. These are spontaneous emission and collisional (nonradiative) quenching by the background gas. We include spontaneous emission through optically allowed transitions, characterized by the Einstein emission coefficients $A_{(n,l)\to(n',l')}$ (s^{-1}).

Rate coefficients for collisional quenching of an excited state are given by $k_Q(n,l)$ $(m^3\ s^{-1})$, which allow optically forbidden transitions of $H(n,l)$ to the ground state and assume uniform depopulation of the available orbitals. Any energy lost to electronic or vibrational excitation is only a few tens of eV and is negligible compared to the keV range of energies considered here. We neglect linear momentum transfer from energetic H to H_2 on the basis that we expect the mean free path for momentum transfer to be larger than the length scale of our discharge. The discharge is taken to be optically thin (emitted light is not reabsorbed).

A rate coefficient k is related to its cross section σ (m^2) through $k(\bar{v})=\int\sigma(v)vf(v,\bar{v})dv$, where v is the relative velocity between interacting particles and $f(v,\bar{v})$ is a relative velocity distribution function parametrized by the mean interaction velocity $\bar{v}$. For energetic atoms or ions interacting with the background gas, v is approximately the atom/ion velocity. Assuming a monoenergetic beam then $f(v,\bar{v})$ is approximated by a δ function such that $k(\bar{v})=\sigma(\bar{v})\bar{v}$. We take the cross sections for charge exchange [15] and quenching [16] to be constant for interactions in units of keV energy range. Values for $A_{(n,l)\to(n',l')}$ (averaged over fine transitions) were obtained from Wiese *et al.* [17].

B. CR model for slow excited H produced by dissociative excitation

The CR model in Ref. [11] considered central peak emission generated by a beam of units of keV electrons with a

monoenergetic electron energy distribution function (EEDF). In this same paper, magnetic deflection of electrons in the interelectrode emission channel showed that they are indeed largely monoenergetic and accelerated to energies in the order of the full applied potential. The model, therefore, neglects the recombination of low-energy secondary electrons as well as any ionizing collisions that would produce them. Rather it was found that the emission is dominated by dissociative excitation of H_2 by fast electrons. We neglect loss of $H_{slow}(n,l)$ due to momentum transfer from atoms with larger kinetic energies. This is based on the assumption that the dissociation fraction f_{slow} of H_2 into $H_{slow}(n,l)$ is small ($f_{slow} \ll 1$) and so momentum transfer is more likely to occur only with the low-energy background gas. Given slow H and small f_{slow}, we also neglect atom-atom (de)excitations as well as interactions between electrons and atoms in excited states.

Rate equations take the form

$$\frac{dn_{H_{slow}(n,l)}}{dt} = k_D(n,l) n_{e^-_{fast}} n_{H_2} - \sum_{\substack{(n',l')<(n,l) \\ \text{allowed}}} A_{(n,l)\to(n',l')} n_{H_{slow}(n,l)}. \tag{7}$$

Here $n_{H_{slow}(n,l)}$ is the number density of slow $H(n,l)$ produced by dissociative excitation of H_2 by fast electrons ($n_{e^-_{fast}}$), with the rate coefficient for this process given by k_D. For a monoenergetic EEDF (that is, a δ function parametrized by the velocity $v_{e^-_{fast}}$ of fast electrons) we may write $k_D = \sigma_D v_{e^-_{fast}}$, where experimental cross sections σ_D for dissociative excitation were obtained from Vroom *et al.* [18].

Unlike the model for charge exchange, each level (n,l) is described by a single equation related to the central peak emission. We note also that the original model had each $n_{H_{slow}(n,l)}$ coupled to higher levels through the inclusion of radiative cascades; however, the removal of this process has a negligible effect on the model output and so is neglected in its present incarnation. We again consider the steady-state case by setting the left-hand side to zero.

C. Absolute densities for fast ions diverging from the cathode

We now use the CR models for fast and slow $H(n=3)$ to relate densities of fast ions and electrons to the H_α spectrum obtained using the setup in Sec. II.

In Refs. [13,14], the Doppler-shifted emission from fast H is interpreted as arising from ions that are created within the cathode and undergo charge exchange as they accelerate away from a central region of positive space charge ("virtual anode"). For ions accelerating to energies of 2–3 kV, the mean free path for charge exchange is 2–3 cm and so we expect $H^x_{fast}(n=3)$ to be produced in the vicinity of the cathode edge. This position corresponds to a minimum in electric potential and a maximum in incident ion velocity. Figure 4 represents this graphically, with energetic Doppler emission at the anode arising from fast excited H produced at the cathode. For Doppler emission measured at an angle $\theta < 90°$ to the discharge passing through the center of the anode ring, we estimate that emitting H travel a distance d_{sep} equal to the axial cathode-anode separation. Combining the observed Doppler shift $\Delta\lambda$ with Eq. (2), we obtain the (approximately monoenergetic) particle energy K and may thus estimate an average time of flight t_{sep}.

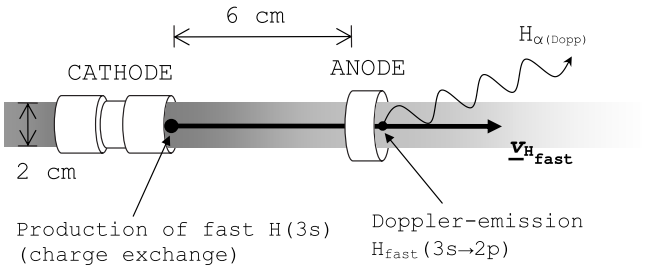

FIG. 4. Graphical depiction of the mechanism for energetic Doppler emission in the IEC discharge.

As $d_{sep} \sim 6$ cm, we are concerned with emission through the channel $3s \to 2p$. This has a radiative lifetime $\tau = 1/A_{3s\to 2p} = 1.6 \times 10^{-7}$ s. For incident H_x^+ of energy 1 keV, this implies a decay length scale $v_H \tau \sim 10$ cm. In contrast, the channels $3p \to 2s$ and $3d \to 2p$ have a decay length on the order of 2 and 1 cm, respectively, and so we neglect emission from fast H in the $3p$ or $3d$ states. We may thus relate the population of $H^x_{fast}(3s)$ at the anode and cathode,

$$n^{anode}_{H^x_{fast}(3s)} = n^{cathode}_{H^x_{fast}(3s)} \exp(-A_{3s\to 2p} t_{sep}). \tag{8}$$

The intensity I_x^{anode} of Doppler emission arising from fast H_x^+ and measured at an angle θ to the emission channel at the anode may then be written

$$I_x^{anode} \propto n^{anode}_{H^x_{fast}(3s)} A_{3s\to 2p} = n^{cathode}_{H^x_{fast}(3s)} A_{3s\to 2p} \exp(-A_{3s\to 2p} t_{sep}). \tag{9}$$

Figure 5 shows the situation for slow $H(n=3)$, where central peak emission at the anode arises through dissociative excitation of H_2 by fast electrons. Since the excited H have negligible kinetic energy ($K \sim 1$ eV), we may assume that unshifted emission occurs at the point in space where the gas is dissociated. The intensity $I^{anode}_{central}$ for central peak emission at the anode is thus given by

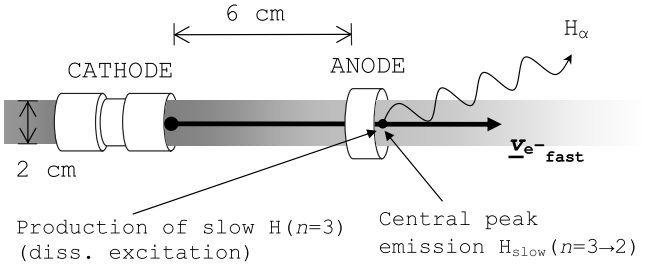

FIG. 5. Graphical depiction of the model for central peak emission produced by dissociative excitation of H_2 by fast monoenergetic electrons.

$$I_{\text{central}}^{\text{anode}} \propto n_{\text{H}_{\text{slow}}(n=3)}^{\text{anode}}(0.16A_{3s\to 2p} + 0.44A_{3p\to 2s} + 0.40A_{3d\to 2p}), \tag{10}$$

where we have used the dissociative excitation branching ratios $(s:p:d)=(16:44:40)$ of Fujimoto *et al.* [19].

As I_x^{anode} and $I_{\text{central}}^{\text{anode}}$ are sampled at equal distances from the respective emitters, at approximately the same wavelength and with the same exposure time and detector slit width, we can neglect any spatial or frequency dependence in their ratio,

$$\frac{I_x^{\text{anode}}}{I_{\text{central}}^{\text{anode}}} = \frac{n_{\text{H}_{\text{fast}}^x(3s)}^{\text{cathode}} A_{3s\to 2p} \exp(-A_{3s\to 2p} t_{\text{sep}})}{n_{\text{H}_{\text{slow}}(n=3)}^{\text{anode}}(0.16A_{3s\to 2p} + 0.44A_{3p\to 2s} + 0.40A_{3d\to 2p})}. \tag{11}$$

Rearranging using the steady-state forms of Eqs. (6) and (7), this becomes

$$\frac{I_x^{\text{anode}}}{I_{\text{central}}^{\text{anode}}} = \frac{n_{\text{H}_x^+}^{\text{cathode}}}{n_{e_{\text{fast}}^-}^{\text{anode}}} \frac{\sigma_x(3s) v_{\text{H}_x^+}^{\text{cathode}}}{\sigma_D(n=3) v_{e_{\text{fast}}^-}^{\text{anode}}} (1+C_1) C_2 \exp(-A_{3s\to 2p} t_{\text{sep}}), \tag{12}$$

where C_1 and C_2 are defined as

$$C_1 = \frac{0.44A_{3p\to 1s}}{(0.16A_{3s\to 2p} + 0.44A_{3p\to 2s} + 0.40A_{3d\to 2p})}, \tag{13}$$

$$C_2 = \frac{A_{3s\to 2p}}{[A_{3s\to 2p} + n_{\text{H}_2}\sigma_Q(3s) v_{\text{H}_{\text{fast}}^x(3s)}]}. \tag{14}$$

We have thus related the density of fast ions emerging from the cathode to the experimental ratio of I_x^{anode} to $I_{\text{central}}^{\text{anode}}$, and also to the density $n_{e_{\text{fast}}^-}^{\text{anode}}$ of fast, monoenergetic electrons at the anode. This method is convenient as the energies of incident ionic species can be read quickly from a single spectrum of H_α using Eq. (2), with the ratio between I_x^{anode} and $I_{\text{central}}^{\text{anode}}$ computed by comparing areas under the respective peaks.

In this work, we estimate electron density by equating the anode current with that measured at the cathode ($I_{\text{anode}} = I_{\text{cathode}}$ by Kirchoff's current law). At the anode, we assume the current is due to a constant flux of electrons (of charge e and mass m_e) streaming from the cathode in a beam of radius r_{beam}. It follows that

$$n_{e_{\text{fast}}^-}^{\text{anode}} = I_{\text{cathode}}/(\pi r_{\text{beam}}^2 e v_{e_{\text{fast}}^-}^{\text{anode}}), \tag{15}$$

where the velocity $v_{e_{\text{fast}}^-}^{\text{anode}}$ of fast, monoenergetic electrons at the anode is calculated by assuming they are accelerated to the full applied potential. Relativistic effects are neglected.

D. Limitations and uncertainties associated with the proposed optical method

Application of the method presented in Sec. III C is restricted to regions of the interelectrode discharge where the electron population is approximately monoenergetic in the units to tens of keV range. This is due to the treatment of the central peak emission; from Ref. [11] we expect that the electron-energy dependence of the central peak intensity is approximated by Eq. (7) only for electron energies greater than about 1.5 keV.

Moreover, some of the experimental and tabulated quantities in Eq. (12) are associated with significant uncertainties. For example, populations of fast ions and neutrals are not perfectly monoenergetic as their respective Doppler peaks can be fit by Gaussians [3–5,13]. This is due not only to convolution with the spectrometer response function but also to the random nature of the charge-exchange process, in which individual ions travel different distances (and accelerate to different energies) before interacting with the gas. We characterize the spread in terms of the Gaussian half-width, which for our discharge is typically about 3 Å. Using Eq. (2), this suggests a spread of energies $\pm(100-300)$ eV for each peak, or about 10–20 % for ions and atoms in the units of keV energy range. In fact, there exist similar uncertainties for the tabulated cross sections for charge exchange and dissociative excitation. We note also that our model assumes all charge exchange occurs at a single point, and that the density of fast ions at this point is given by $n_{\text{H}_x^+}$. In reality, however, charge exchange will occur for a range of positions along and about the discharge axis.

For 2–3 keV ions traveling through a 20 mTorr gas, the mean free path length for charge exchange is in the order 2–3 cm (similar to the half-length of the cathode). We therefore assume an axial "interaction range" smaller than ± 1 cm on either side of the cathode edge, which would introduce an uncertainty up to 15% in the time of flight t_{sep}. As a result of all these combined uncertainties, absolute densities $n_{\text{H}_x^+}^{\text{cathode}}$ computed using Eq. (12) are best interpreted as order-of-magnitude estimates, averaged over space in the vicinity of the cathode edge.

Finally, our treatment of the anode current ignores other parts of the discharge, for example, the low intensity emission surrounding the outer surface of the cathode. As a result, we may overestimate the anode current—and thus the densities of fast electrons and ions—by some small, unknown fraction.

E. Densities of in-falling ions at the anode

The model presented in Sec. III assumes that the majority of ions are created within the cathode, but also permits the existence of slow (10–100 eV) ions created by fast electrons at the anode. Our spectroscopic method may be applied to these ions by considering the resultant Doppler-shifted emission in the vicinity of the anode.

To this end, we modify Eq. (9) to consider Doppler-shifted emission at the anode resulting from slow ions accelerating toward the cathode. This amounts to replacing $n_{\text{H}_{\text{fast}}^x(3s)}^{\text{anode}}$ with $n_{\text{H}_{\text{slow}}^x(n=3)}^{\text{anode}}$ and assuming equal production into the $3s$, $3p$, and $3d$ states. The latter assumption is appropriate as the emitting neutral atoms have low energies and travel only a short distance ($\lesssim 1$ cm) before emitting, meaning we cannot isolate emission arising through the various fine tran-

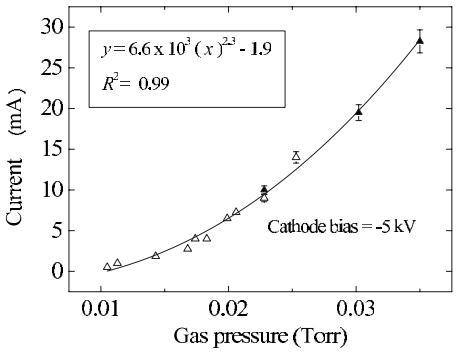

FIG. 6. Cathode current versus pressure (bias −5 kV). Filled and hollow data points indicate separate experimental runs, with the solid curve showing a numerical fit.

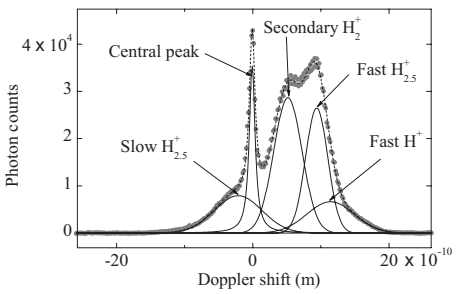

FIG. 7. Typical spectrum (discrete points) observed at $\theta=25°$ to the emission channel through the center of the anode ring. We label the Lorentzian fitted to the central peak as well as Gaussians for red- and blueshifted Doppler peaks. The dashed curve represents the total fit.

sitions. Equation (9) for Doppler-shifted emission is thus replaced by

$$I_x^{\text{anode}} \propto n_{\mathrm{H}^x_{\text{slow}}(n=3)}^{\text{anode}}\left[\tfrac{1}{3}(A_{3s\to 2p}+A_{3p\to 2s}+A_{3d\to 2p})\right], \quad (16)$$

whereas Eq. (10) for central peak emission remains unchanged. In the counterpart to Eq. (12), the modification involves replacing $n_{\mathrm{H}_x^+}^{\text{cathode}}$ with $n_{\mathrm{H}_x^+}^{\text{anode}}$, $v_{\mathrm{H}_x^+}^{\text{cathode}}$ with $v_{\mathrm{H}_x^+}^{\text{anode}}$, and using the total H($n=3$) production cross section $\sigma_x(n=3)$ for charge exchange (C_2 is redefined here also). The modified expressions are

$$\frac{I_x^{\text{anode}}}{I_{\text{central}}^{\text{anode}}} = \frac{n_{\mathrm{H}_x^+}^{\text{anode}}}{n_{e^-_{\text{fast}}}^{\text{anode}}}\frac{\sigma_x(n=3)v_{\mathrm{H}_x^+}^{\text{anode}}}{\sigma_D(n=3)v_{e^-_{\text{fast}}}^{\text{anode}}}(1+C_1)C_2, \quad (17)$$

$$C_2 = \frac{\tfrac{1}{3}(A_{3s\to 2p}+A_{3p\to 2s}+A_{3d\to 2p})}{\left[\tfrac{1}{3}(A_{3s\to 2p}+A_{3p\to 2s}+A_{3p\to 1s}+A_{3d\to 2p})+n_{\mathrm{H}_2}\sigma_Q(n=3)v_{\mathrm{H}_x^+}\right]}. \quad (18)$$

In analyzing H_α spectra for an experimental IEC discharge, we may now compare density estimates for fast ions emerging from the cathode to those of slow ions accelerating away from the anode.

IV. RESULTS AND DISCUSSION

In this section, we describe the measurement of central and Doppler peak emission intensities for the experimental IEC discharge detailed in Sec. II. The methods developed in Secs. III C and III E are used to determine absolute population densities for energetic ions emerging from the cathode as well as slow ions at the anode.

A. Measurement of central- and Doppler-peak intensities

Keeping the cathode bias constant at −5 kV and with cathode currents in the range 1–30 mA, we recorded several H_α spectra at an angle $\theta=25°$ to the emission channel through the center of the anode ring. Cathode current was varied by adjusting gas pressure in the range 10–30 mTorr, where the variation may be fit by a power law (Fig. 6).

Spectra were recorded for eight values of current across two separate trials (sets 1 and 2 are denoted by filled and hollow data points, respectively). All measurements used identical parameters for the detector setup (10×5000 ms exposures with a constant slit width 20 μm). A typical spectrum is shown in Fig. 7.

The intensity of the Doppler redshifted emission is greater than for the blueshifted wing, with the red peak also extending out to larger Doppler shift magnitudes. Given the line of sight of our detector with respect to the electrode arrangement [Fig. 3(b)], this suggests the incident fast ions are traveling toward the anode ring. In Fig. 7, the central peak intensity is associated with the area of a Lorentzian fitted using a commercial software package (ORIGIN). Following the same procedure as in Refs. [3–5,13], emission intensities associated with the energetic redshifted charge-exchange peaks are measured by fitting three Gaussians, also labeled in the figure. Energies for the incident ionic species are assumed to be approximately monoenergetic and are determined by using Eq. (2) with the observed Doppler shift $\Delta\lambda$ for a given peak maximum.

It has been shown [13,14] that for pressures in the tens of mTorr range, the peaks associated with H_2^+ and H_3^+ are not resolved but instead form a merged peak. Moreover, these species are expected to be present in approximately equal numbers [5], and so for this peak (labeled "Fast $\mathrm{H}_{2.5}^+$") we assume an average incident ion mass of $2.5\times m_{\mathrm{H}}$. Here the red peak closest to the central peak is associated with sec-

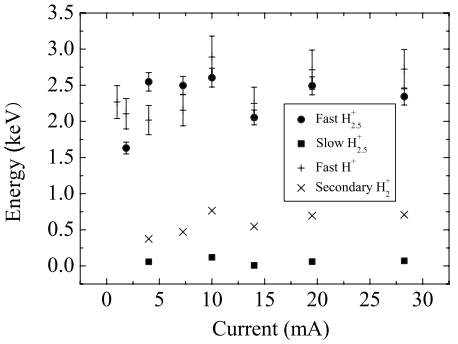

FIG. 8. Incident ion energies for the charge-exchanging species identified in Fig. 7. For clarity, we do not distinguish between experimental runs.

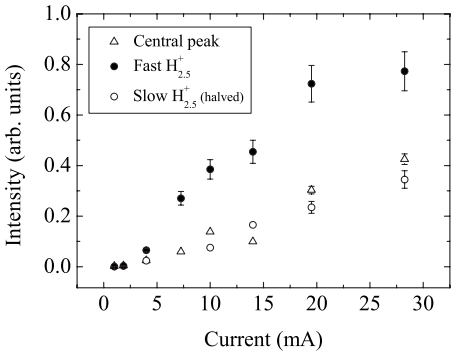

FIG. 9. Intensity (arbitrary units) for the various emission peaks identified in Fig. 7. For slow in-falling $H^+_{2.5}$, the raw intensities have been halved (see text). We do not distinguish between experimental runs.

ondary charge-exchange interactions arising from low-energy (hundreds of eV) H_2^+, which are produced in the energetic processes of Eqs. (3)–(5) and accelerate back and forth through the potential minimum in the vicinity of the cathode edge. The low energy (10–100 eV) blueshifted Gaussian in Fig. 7 is associated with slow $H_{2.5}^+$ produced at the anode.

Figure 8 shows the incident ion energies associated with the energetic H^+ and $H_{2.5}^+$ Doppler peaks, as well as the redshifted secondary peak and low energy blueshifted peak. We note that the energies for fast H^+, and $H_{2.5}^+$ agree to within 25% across the range of pressures and currents. This suggests the energetic peaks have been identified correctly; all fast species are thought to accelerate away from the same region of space charge within the cathode, and so should acquire similar energies.

The energies for lower energy blue- and redshifted peaks have large uncertainties due to their close proximity to the background noise level (in fact, we were not able to identify these peaks in all of the spectra). Taking into account fitting errors for the peak centers (20% for slow $H_{2.5}^+$, 10% for fast H^+, and 5% for fast $H_{2.5}^+$ and redshifted secondary H_2^+), then the energies for fast H^+ and $H_{2.5}^+$ are about 50% of the applied cathode potential. This is similar to Doppler and Langmuir probe measurements performed by Khachan *et al.* [4] with a cylindrically symmetric two-ring cathode. The only exception is at the lower bound of our current range, where the fast H^+ peak was nearly indistinguishable from the background.

In Fig. 9, we plot the intensities for the peaks associated with fast $H_{2.5}^+$ emerging from the cathode, slow $H_{2.5}^+$ at the anode, and central peak emission, where uncertainties are estimated using the fitting errors. Intensity for each peak increases roughly linearly with current over the 10–30 mA range. Note that for slow $H_{2.5}^+$ we have halved the raw intensities. Paradoxically, this is because the Gaussian fitting procedure places almost half of the blueshifted Gaussian in the redshifted part of the spectrum. Nevertheless, the halved intensities coincide with those for the central peak. In some sense we expect this to be the case as slow ions at the anode are thought to be created by the same fast electrons responsible for unshifted emission.

The ratios of Doppler ($x \sim 2.5$) to central peak emission versus current are shown in Fig. 10 (variation with pressure is similar). Intensity ratios are in the range 1–5 for currents greater than 2.5 mA; however, there exists significant variation between trials. In the next section, we apply the method of Sec. III C to extract additional information.

B. Determination of densities for fast ions emerging from the cathode

Using the intensity measurements of Sec. IV A and assuming the model of Ref. [13], we apply Eqs. (12)–(14) in order to calculate the ratios of fast $H_{2.5}^+$ emerging from the cathode to fast electrons at the anode. These are the circular data points in Fig. 11. The calculations assume incident ion energies 50% of the applied bias, and approximate a charge exchange cross section for $x=2.5$ by averaging the cross sections for $x=1,3$. Error bars are not shown as we expect the calculated values to represent order-of-magnitude estimates only (see Sec. III D). For increasing current, the density ratio appears either to approach an asymptote or to decrease following a maximum in the order $\sim$100–200.

The ratios $n_{H_{2.5}^+}^{\text{cathode}}/n_{e^-_{\text{fast}}}^{\text{anode}}$ are combined with Eq. (15) for electron densities using a beam radius $r_{\text{beam}} \sim 1$ cm. We arrive at this value by observing electron beam fluorescence of the glass vacuum chamber, noting that r_{beam} is in the order of the cathode radius (which supports the assumption of a cylindrical discharge). The radius is largely invariant with cur-

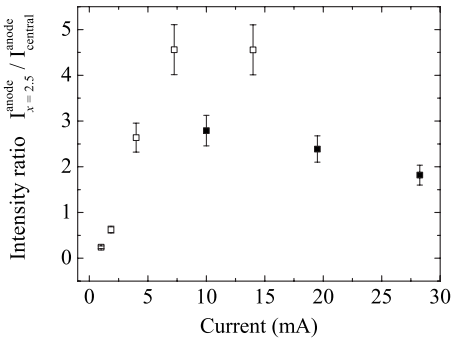

FIG. 10. Intensity ratios of energetic Doppler ($x \sim 2.5$) to central peak emission versus current. Filled and hollow points indicate separate experimental runs.

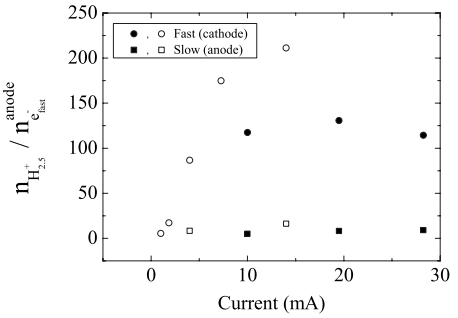

FIG. 11. Relative population densities of ions to fast electrons at the anode. Circles refer to fast $H_{2.5}^+$ at the cathode. Squares refer to slow $H_{2.5}^+$ at the anode. Filled and hollow data points indicate different experimental runs.

rent as our hollow cathode discharge is in the abnormal mode, where current and bias are strongly proportional to one another. The resulting absolute densities for fast $H_{2.5}^+$ emerging from the cathode are shown by the circular data points in Fig. 12.

For currents in the range 5–25 mA, fast ion densities exhibit a roughly linear increase from 10^8–10^9 cm^{-3}. This is in agreement with values inferred by measuring the ion drag force on dust particles sprinkled through the emission channel of a similar apparatus [20]. For currents in the range 5–25 mA, there is also an approximate proportionality between the intensity of fast Doppler peaks and the corresponding absolute ion densities (cf. Figs. 9 and 12). This is in agreement with the model of Ref. [13], where a linear increase of energetic Doppler emission with current would be attributed to a similarly linear increase in the flux of fast ions emerging from the cathode.

We use the modified Eqs. (17) and (18) to calculate density estimates for slow (~100 eV) ions created at the anode (square data points in Fig. 12). We find that the absolute densities are about an order of magnitude lower than for fast ions at the cathode edge. Neglecting the loss of ions due to charge exchange between the anode ring and a surface "CX" defining the mean position of charge exchange, we can then relate the ion density n and velocity v at the two surfaces by writing $(nv)^{\text{anode}}_{H_{2.5}^+}=(nv)^{\text{CX}}_{H_{2.5}^+}$. As a result, if slow $H_{2.5}^+$

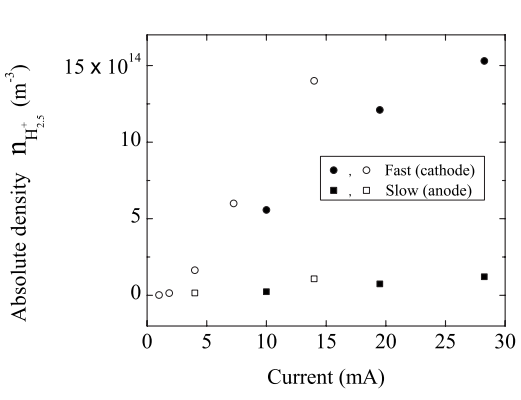

FIG. 12. Absolute densities for fast $H_{2.5}^+$ in the vicinity of the cathode edge (circles), and slow $H_{2.5}^+$ at the anode (squares). Filled and hollow data points indicate different experimental runs.

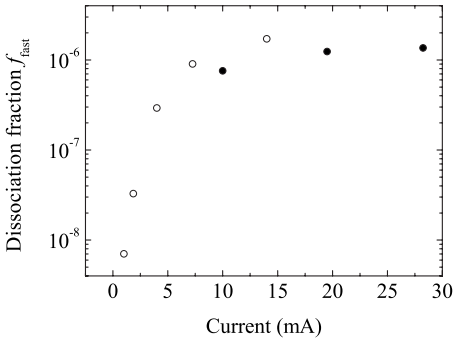

FIG. 13. Dissociation fraction f_{fast} of the background gas into fast $H_{2.5}^+$ at the cathode.

accelerate from 100 to 2500 eV between the anode ring and the surface CX, we expect their density to decrease by about an order of magnitude, which is about 100 times smaller than the densities of fast ions emerging from the cathode. This too is consistent with the model of Ref. [13], where fast ions beginning their acceleration at the anode ring are thought to comprise a lesser component of the discharge.

Finally, in combining the data of Figs. 6 and 12, we calculate the dissociation fraction $f_{\text{fast}}=n^{\text{cathode}}_{H_{2.5}^+}/n_{H_2}$ of the background gas into fast $H_{2.5}^+$ at the cathode (see Fig. 13). For currents greater than 10 mA, we find that $f_{\text{fast}}\sim(1-2)\times10^{-6}$ and is largely independent of current. In a similar discharge of deuterium, the parameter f_{fast} is of use in predicting the rate $R_{\text{D-D}}$ of D-D fusion reactions. These are related through

$$R_{\text{D-D}}=n_{D^+_{\text{fast}}}n_{D_2}\sigma_{\text{D-D}}v_{D^+_{\text{fast}}}=f_{\text{fast}}(n_{D_2})^2\sigma_{\text{D-D}}v_{D^+_{\text{fast}}},$$

where $n_{D^+_{\text{fast}}}$ is the population density of fast monoenergetic deuteron ions (of velocity $v_{D^+_{\text{fast}}}$), n_{D_2} is the density of the deuterium gas, and $\sigma_{\text{D-D}}$ is the cross section for neutron production. As the deuteron has emission characteristics similar to that of atomic hydrogen, we can apply the same spectroscopic method we have employed here, adjusting only the rate coefficients for dissociative excitation of D_2 and charge exchange of fast D ions. We note that our chosen cathode bias (−5 kV) is an order of magnitude smaller than that seen in typical IEC neutron production applications. This was appropriate given our experimental apparatus and available hydrogen cross-section data; however, future work will aim to calibrate this method by comparing values of f_{fast} obtained through emission and nuclear spectroscopy (in D_2) for larger magnitudes of cathode bias.

V. CONCLUSIONS

We developed an optical measurement for absolute densities of fast (units to tens of keV) hydrogen ions emerging from a cylindrically symmetric hollow cathode operating in the abnormal mode at units to tens of mTorr pressures. CR models for central- and energetic Doppler-shifted emission were combined, with the resulting method requiring only a single spectrum of Balmer H_α emission, along with some estimate of the density of fast electrons. Limitations of the

method are a large associated uncertainty for the density values (order-of-magnitude estimates only), and a requirement that measurements be made in a region where the electron population is roughly monoenergetic.

We applied this method in calculating the densities of fast ions in the vicinity of the cathode edge in a cylindrically symmetric inertial electrostatic confinement (IEC) device. This was achieved by observing several spectra of H_α at an angle $\theta < 90°$ to one of the characteristic emission channels at the anode. Our calculated densities were in the order $(1-10)\times 10^{14}$ m^{-3}, which agree with values inferred using Langmuir probes [3] and analysis of dust particle motion [20] in similar apparatus. These results support the model of Ref. [13], which suggests that the dominant component of energetic Doppler emission arises from fast ions emerging from the cathode.

The absolute densities were also used to calculate the dissociation fraction of background gas into fast ions at the cathode. In a similar discharge of deuterium, knowledge of the dissociation fraction allows calculation of nuclear fusion rates, and so this result suggests a means by which our method may be further validated.

[1] W. Benesch and E. Li, Opt. Lett. **9**, 338 (1984).
[2] E. L. Ayers and W. Benesch, Phys. Rev. A **37**, 194 (1988).
[3] J. Khachan and S. Collis, Phys. Plasmas **8**, 1299 (2001).
[4] J. Khachan, D. Moore, and S. Bosi, Phys. Plasmas **10**, 596 (2003).
[5] M. Fitzgerald, J. Khachan, and S. Bosi, Eur. Phys. J. D **39**, 35 (2006).
[6] M. Adamov, B. Obradović, M. Kuraica, and N. Konjević, IEEE Trans. Plasma Sci. **31**, 444 (2003).
[7] G. Baravian, Y. Chouan, A. Ricard, and G. Sultan, J. Appl. Phys. **61**, 5249 (1987).
[8] C. Barbeau and J. Jolly, J. Phys. D **23**, 1168 (1990).
[9] G. McClure, Phys. Rev. **140**, A769 (1965).
[10] R. McWhirter, *Plasma Diagnostic Techniques* (Academic, New York, 1965).
[11] J. Kipritidis, M. Fitzgerald, and J. Khachan, J. Phys. D **40**, 5170 (2007).
[12] R. L. Hirsch and G. A. Meeks, U.S.Patent No. 3,530,497 (1970).
[13] O. Shrier, J. Khachan, S. Bosi, M. Fitzgerald, and N. Evans, Phys. Plasmas **13**, 012703 (2006).
[14] O. Shrier, J. Khachan, and S. Bosi, J. Phys. A **39**, 11119 (2006).
[15] A. Phelps, J. Phys. Chem. Ref. Data **19**, 653 (1990).
[16] M. Wouters, J. Khachan, I. Falconer, and B. James, J. Phys. B **32**, 2869 (1996).
[17] W. Wiese, M. Smith, and B. Glennon, *Atomic Transition Probabilities: Hydrogen through Neon. A Critical Data Compilation*, NSRDS-NBS 4 (National Bureau of Standards, Washington, D.C., 1966).
[18] D. Vroom and F. D. Heer, J. Chem. Phys. **50**, 580 (1969).
[19] T. Fujimoto, K. Sawada, and K. Takahata, J. Appl. Phys. **66**, 2315 (1989).
[20] J. Khachan and A. Samarian, Phys. Lett. A **363**, 297 (2006).